Materials Science and Engineering B 176 (2011) 660–668

Contents lists available at ScienceDirect

Materials Science and Engineering B

journal homepage: www.elsevier.com/locate/mseb

Effects of laser scans on the diffusion depth and diffusivity of gallium in n-type 4H–SiC during laser doping

Geunsik Lim, Aravinda Kar*

Laser-Advanced Materials Processing Laboratory, Department of Mechanical, Materials and Aerospace Engineering, College of Optics and Photonics, Center for Research and Education in Optics and Lasers (CREOL), University of Central Florida, Orlando, FL 32816-2700, USA

ARTICLE INFO

Article history:
Received 18 November 2010
Received in revised form 6 February 2011
Accepted 16 February 2011

Keywords:
Laser doping
Silicon carbide
Diffusion coefficient
Gallium dopant

ABSTRACT

An n-type 4H–SiC substrate has been doped with gallium using a continuous wave Nd:YAG laser to heat the sample to high temperatures but below the peritectic temperature of SiC. Mathematical models have been presented for the temperature and Ga concentration distributions in the sample. The Ga atoms, which are produced due to the thermal decomposition of a metallorganic precursor, diffuse into the sample by the solid-phase diffusion process at high temperatures. This process is modeled by considering the temperature-dependent diffusion coefficient and the Ga concentration profile was measured by the secondary ion mass spectrometry (SIMS). The concentration of Ga (6.25×10^{20} cm^{-3}) at the substrate surface was found to exceed the solid solubility limit (1.8×10^{19} cm^{-3}) of Ga in SiC. Comparing the SIMS data to the results of the diffusion model, the activation energy, pre-exponential factor and diffusion coefficient of Ga were determined for different doping conditions. Four doped samples were produced by scanning the samples with a laser beam for different number of passes. The sample prepared with four passes showed the highest diffusion coefficient of 5.53×10^{-7} cm^2/s with activation energy 1.84 eV and pre-exponential factor 1.05×10^{-2} cm^2/s. The diffusion coefficient is five orders of magnitude higher than the typical diffusion coefficient of Ga in SiC. This indicates that the laser doping process enhances the diffusion coefficient of dopant significantly.

1. Introduction

Silicon carbide (SiC) has numerous polytypes and the most commonly available phases are the cubic (3C–SiC) and hexagonal (6H–SiC and 4H–SiC) crystal structures. Crystalline SiC is an attractive material for modern electronics involving high temperature, high frequency, and high power device applications due to its high thermal conductivity (4.9 W/cm K), high melting temperature (3100 K peritectic temperature), high breakdown field (3–5 MV/cm), and very good radiation- and oxidation-resistant properties [1,2]. However some of the thermochemical properties of SiC, such as high melting point, very good thermal and chemical stability and very low diffusion coefficient of impurities, cause the incorporation and activation of dopants in SiC by the conventional thermal diffusion process extremely difficult. Many dopant atoms occupy the interstitial positions in the lattice during the diffusion process and they must be transferred to the substitutional sites to create electrically active doped sites. The conventional solid state diffusion process, which occurs under an isothermal condition in a furnace to form diffused layers of impurities, is inappropriate for diffusion at high activation energies (1.29–2.69 eV) in SiC [2]. The laser doping technique is a nonisothermal solid state diffusion process in which the substrate is not melted and the diffusion can be carried out at much higher temperatures than in the conventional diffusion process. This nonisothermal, high temperature diffusion mechanism enhances the dopant diffusion coefficient.

Usually the dopant diffusion coefficients are very low in ion-implanted substrates. The diffusion coefficient of B in SiC was found to be 4.38×10^{-14} cm^2/s for which transient and field-enhanced diffusion of implanted B was proposed for the migration of B within 4H–SiC [3–5]. A lower limit was determined to be 7.0×10^{-12} cm^2/s for the effective diffusion coefficient of B at 1600 °C. Usov et al. [5] reported very low diffusion coefficient of Al in SiC as 2.0×10^{-15} cm^2/s at 1700 °C, pointed out that the structure of the implanted layer may have a strong effect on the redistribution of Al and proposed a dissociative diffusion mechanism during the high-temperature implantation. The ion implantation process causes significant lattice damage. In spite of annealing the implanted samples at extremely high temperatures (1400–1700 °C) for redistributing and activating the dopants, a large fraction of the implanted ions remains at the interstitial sites, resulting in poor electrical activity. Laser doping was examined as a promising alternative technique because of its several advantages [6–10]. It can be carried out at room temperature ambient,

* Corresponding author. Tel.: +1 407 823 6921; fax: +1 407 823 6880.
E-mail address: akar@creol.ucf.edu (A. Kar).

0921-5107/$ – see front matter © 2011 Elsevier B.V. All rights reserved.
doi:10.1016/j.mseb.2011.02.011

unlike the large volume heating in furnace-based doping, by heating only the doped region to a high temperature with a laser beam. This localized heating was utilized to demonstrate doping from gas or solid precursor [11–13] and annealing of ion-implanted SiC [14].

Forming shallow junctions, particularly *p+* shallow junctions, is difficult by the conventional ion implantation technique due to the lack of controlling low energy ion beams precisely. Doping techniques were developed using excimer lasers to form very shallow junctions in silicon wafers [15–17]. Silicon absorbs excimer lasers strongly in the near-surface region due to its large absorption coefficient. So the pulsed laser can heat up a very thin surface layer to high temperatures and produce a shallow doped region with solid phase dopant solubility much higher than those obtained by the conventional isothermal diffusion process.

Polytype phase transitions were observed in ion-implanted SiC crystals annealed at high temperatures [18,19]. Such phase transitions are not desirable for electronic devices. At high temperatures, most common metals or metal silicides used in modern device fabrication melt and the properties of most common dielectrics such as SiO_2 change. Laser annealing is considered to prevent the polytype phase transition since the implanted layer is heated to the annealing temperature within a very short (50–150 ns) laser pulse, inducing rapid heating and cooling of the layer [19].

Tian et al. [20,21] studied the diffusion of nitrogen and aluminum in SiC using pulsed excimer and Nd:YAG lasers. They presented a diffusion model based on temperature-averaged diffusion coefficient by dividing the dopant concentration profile into two distinct regions, near-surface and far-surface regions. For these two regions, they determined the effective diffusion coefficients as 2.4×10^{-5} and 9.2×10^{-6} cm^2/s for nitrogen and 1.2×10^{-5} and 1.3×10^{-6} cm^2/s for aluminum, respectively, which are six orders of magnitude higher than the typical values for these two dopants in SiC. Bet et al. [22] examined the effects of the laser electromagnetic field and thermal stresses on the dopant diffusion during laser doping. They doped SiC with Cr and reported its effective diffusion coefficients as 4.61×10^{-10} cm^2/s at 2898 K and 6.92×10^{-12} cm^2/s at 3046 K for 6H–SiC and 4H–SiC, respectively [22], and demonstrated that almost all of the Cr atoms were in their electrically activated state [23]. They also analyzed the surface roughness and crystalline quality of the laser-doped sample by atomic force microscopy and high resolution transmission electron microscopy, respectively, and demonstrated that the laser-doping process did not damage the substrate surface and crystalline order of the sample.

In this paper, Ga atoms are incorporated into n-type 4H–SiC using a continuous wave (CW) Nd:YAG laser of wavelength 1064 nm and the dopant concentration profiles were measured using secondary ion mass spectrometry (SIMS). A CW laser heating model is presented to determine the temperature distribution in the SiC substrate during the laser doping process, whereas the previous studies [21,22] considered pulsed laser heating. The dopant concentration profile is determined theoretically by considering spatially varying temperature-dependent diffusion coefficient in a diffusion model, which differs from the previous models [21,22] where the dopant profiles were divided into two regions and the temperature was considered constant in each region. Therefore the present model enables fitting the experimental dopant profile with a single theoretical curve. Comparing the SIMS data to the model predictions, the pre-exponential factor and activation energy for the diffusion of Ga are determined. The substrate was scanned with different number of laser passes to control the dopant concentration profile in order to study the effect of laser passes on the diffusion coefficient, which was not investigated in previous studies.

2. Sample preparation, laser doping experiment and dopant concentration profile

An n-type 4H–SiC substrate of length, width and thickness 10, 10 and 0.375 mm, respectively, was cleaned by soaking it in H_2O_2:H_2SO_4 (1:1 by volume) solution for 15 minutes. It was then rinsed with de-ionized water and dipped into buffered oxide etchant. The clean substrate was placed in a chamber of 1 mTorr vacuum. The experimental laser doping setup is shown in Fig. 1. A bubbler containing triethylgallium ($(C_2H_5)_3Ga$) was used to dope the substrate. The precursor vapor was produced by placing the bubbler in a water bath of temperature 100 °C and the vapor was carried to the vacuum chamber with a carrier gas Ar. The substrate was simultaneously heated with a CW Nd:YAG laser to produce Ga atoms by thermal decomposition of the precursor vapor at the laser-heated spot and to induce the diffusion of Ga atoms into the substrate. A laser beam of power 10.5 W was delivered to the substrate with a lens of focal length 150 mm to create a laser spot of diameter 200 μm on the substrate surface. The laser beam scanning was achieved by moving the substrate at the speed of 0.8 mm/s in the *x* direction with an *x*–*y* translation stage (Fig. 2). After scanning a distance of 3 mm, the substrate was moved in the *y* direction and the scanning was repeated in the *x* direction. This cycle was continued to produce a doped region of length 3 mm and width 3 mm in quadrant 1 at the top surface of the substrate (Fig. 2). Similarly the other three quadrants (2, 3, 4 in Fig. 2) were doped by varying the number of laser passes. The substrate was at room temperature at the starting moment of each scan in the *x* direction.

After the doping experiment, the sample was cleaned with a KOH (45 wt.%) solution and then rinsed with acetone, methanol and de-ionized water to carry out SIMS studies. The dopant depth and concentration distribution were measured using a PHI Adept 1010 Dynamic SIMS system with O_2^+ sources forming the primary ion beam of current 200 nA and voltage 5 kV. All measurements were performed under the following conditions, raster size 200 μm, depth resolution 1 nm, mass resolution 100 amu, mass range 0–340 amu, quadrupole mass analyzer, and the detection area was 5% of the raster area. With these conditions, the analyzed area is estimated to be 200 μm × 200 μm.

3. Mathematical models

3.1. Thermal model for temperature distribution in SiC during laser doping

The density of phonons, i.e., the random vibrational motions of the Si, C and Ga atoms, depends on the temperature of the substrate. Thus the temperature affects the diffusion of dopant atoms in the substrate. The laser-induced temperature distribution can be estimated by solving the heat conduction equation for a given doping condition. In the present case, the optical properties of the n-type SiC substrate at the wavelength of the laser are such that the substrate reflects the incident laser beam partially and absorbs it partially as the laser beam propagates through the substrate. The absorption occurs due to the interaction between the laser beam and the free carriers of the n-type substrate, resulting in a volumetric source of thermal energy for heating the substrate. Since the laser beam moves relative to the substrate, the heating process involves three-dimensional, transient heat conduction with advection. To simplify the thermal analysis in this study, the following one-dimensional, transient heat conduction equation is considered because most of the heat conducts in one direction along the thickness of the substrate:

$$k\frac{\partial^2 T(z,t)}{\partial z^2} + S(z) = \rho C_P \frac{\partial T(z,t)}{\partial t}, \quad (1)$$

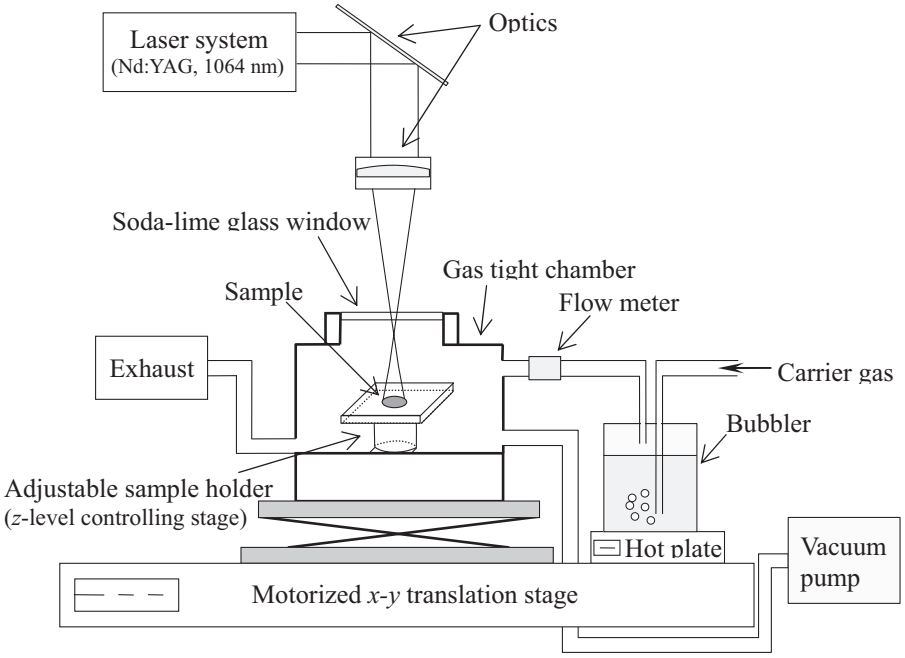

Fig. 1. Experimental setup for laser doping of n-type 4H–SiC with Ga.

where k, ρ and C_P are the thermal conductivity, density and specific heat capacity at constant pressure of the 4H–SiC substrate, respectively, and $T(z,t)$ represents the temperature of the substrate at any depth z (Fig. 2) and time t. $S(z)$ is the volumetric heat source given by [24,25] $S(z) = I_0\mu(1-R)e^{-\mu z}$ for a laser beam propagating in the z direction, where I_0 is the laser irradiance at the substrate surface, μ is the absorption coefficient of the substrate and R is its reflectance. The boundary and initial conditions for Eq. (1) are given by

$$\frac{\partial T}{\partial z} = 0 \quad \text{at} \quad z = 0, \tag{2a}$$

$$-k\frac{\partial T}{\partial z} = h(T - T_\infty) \quad \text{at} \quad z = d, \tag{2b}$$

$$T(z, 0) = T_i, \tag{2c}$$

where h is the heat transfer coefficient, T_∞ is the ambient temperature inside the vacuum chamber far away from the bottom surface of the substrate, d is the substrate thickness and T_i is its initial temperature. Defining a set of dimensionless variables as $T_1(z_1, t_1) = (T(z, t) - T_\infty)/[(1-R)I_0\mu d^2/k]$, $z_1 = z/d$ and $t_1 = t/\tau$, where τ is the laser-substrate interaction time given by the ratio of the laser beam diameter to the laser scanning speed relative to the substrate, and letting $T_1(z_1, t_1) = \theta(z_1, t_1) + e^{-\mu_1 z_1}/\mu_1^2 - z_1/\mu_1 + (1 + Bi)/\mu_1 - (1 - \mu_1 Bi)e^{-\mu_1}/\mu_1^2$ where $\mu_1 = \mu d$ and Bi is the Biot number given by $Bi = hd/k$. Eq. (1) and the boundary and initial conditions (Eqs. (2a)–(2c)) can be written as follows

$$\frac{\partial^2\theta(z_1, t_1)}{\partial z_1^2} = \frac{1}{Fo}\frac{\partial\theta(z_1, t_1)}{\partial t_1}, \tag{3}$$

where Fo is the Fourier number, $Fo = \alpha\tau/d^2$, and α is the thermal conductivity, $\alpha = k/\rho C_P$,

$$\frac{\partial\theta(z_1, t_1)}{\partial z_1} = 0 \quad \text{at} \quad z_1 = 0, \tag{4a}$$

$$-\frac{\partial\theta(z_1, t_1)}{\partial z_1} = Bi\theta(z_1, t_1) \quad \text{at} \quad z_1 = 1, \tag{4b}$$

and

$$\theta(z_1, 0) = \frac{T_i - T_\infty}{I_0\mu d^2(1-R)/k} - \frac{e^{-\mu_1 z_1}}{\mu_1^2} + \frac{z_1}{\mu_1} - \frac{1 + Bi}{\mu_1} + \frac{(1 - \mu_1 Bi)e^{-\mu_1}}{\mu_1^2}. \tag{4c}$$

Eq. (3) can be solved by the method of separation of variables to obtain the temperature distribution as

$$T(z, t) = T_\infty + \frac{(1-R)I_0\mu d^2}{k} \times \left[\sum_{n=1}^{\infty}\left[\frac{(T^* - A_2)f_2 - A_1 f_3 - f_4/\mu_1^2}{f_1} \times \cos(\lambda_n z_1)B_3 e^{-\lambda_n{}^2 Fo t_1} + \frac{1}{(\mu_1)^2}e^{-\mu_1 z_1} - \frac{z_1}{\mu_1} + \frac{1}{\mu_1}\{1 + Bi\} - \frac{e^{-\mu_1}}{\mu_1}\left\{\frac{1}{\mu_1} - Bi\right\}\right], \tag{5}$$

where the eigenvalues, λ_n, are obtained by solving the transcendental equation $\lambda_n \tan(\lambda_n) = Bi$, and f_1, f_2, f_3 and f_4 are

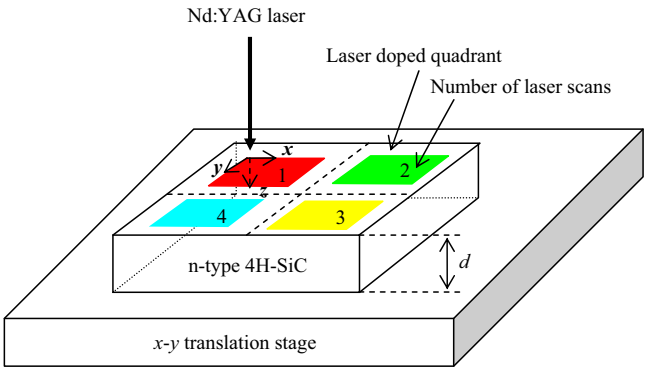

Fig. 2. Doped quadrants of dimensions 3 mm × 3 mm each for different number of laser scans.

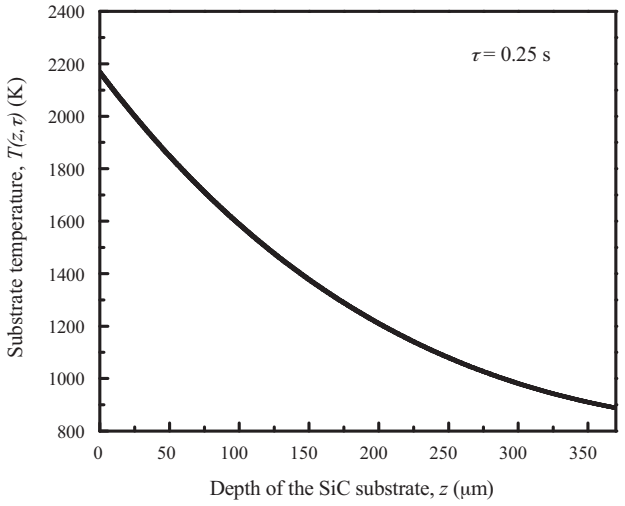

Fig. 3. Temperature distribution along the depth of the substrate during laser doping for 4 laser passes.

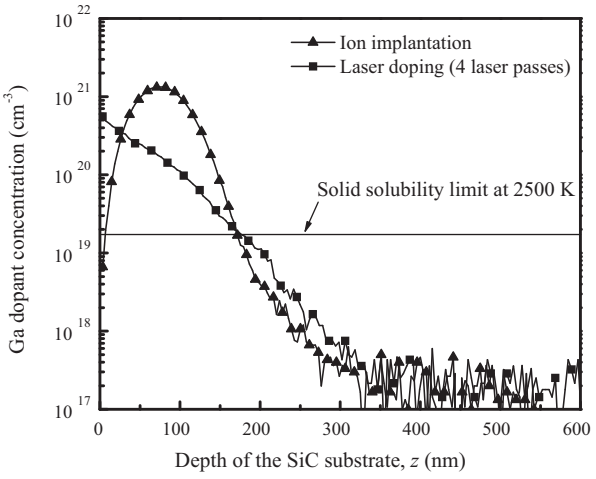

Fig. 5. Ga dopant concentration obtained by converting the original SIMS data from the arbitrary unit to cm^{-3} using an ion-implanted n-type 4H–SiC standard.

given by $f_1 = (Bi + \lambda_m^2 + Bi^2)/2(\lambda_m^2 + Bi^2)$, $f_2 = \sin(\lambda_m)/\lambda_m$, $f_3 = -1/\lambda_m^2 + (1 + Bi)\cos(\lambda_m)/\lambda_m^2$ and $f_4 = [\mu_1 + (Bi - \mu_1)e^{-\mu_1 z_1}\cos(\lambda_m z_1)]/(\mu_1^2 - \lambda_m^2)$. The temperature distribution, $T(z,t)$, is obtained from Eq. (5) and used in the following diffusion model to determine the temperature-dependent diffusion coefficient of Ga in SiC during laser doping.

3.2. Diffusion model with temperature-dependent diffusion coefficient for dopant concentration distribution

Due to the localized heating capability of lasers with precise control on energy delivery, the substrate can be heated to very high temperatures for doping different regions selectively without any melting. The temperature varies along the depth of the substrate, providing a nonisothermal mechanism for the diffusion of dopant atoms. Also high temperatures represent high energy states for the random vibrational motions of the atoms, which can facilitate the migration of dopants. The dopant concentration distribution is modeled using the following one-dimensional, transient diffusion equation [26]:

$$\frac{\partial}{\partial z}\left[D_0 e^{-Q/k_B T(z,\tau)}\frac{\partial C(z,t)}{\partial z}\right] = \frac{\partial C(z,t)}{\partial t}, \quad (6)$$

where D_0, Q and k_B are the pre-exponential factor, activation energy per atom and the Boltzmann constant, respectively. $D_0 e^{-Q/k_B T(z,\tau)}$ is the temperature-dependent diffusion coefficient of Ga in 4H–SiC, where $T(z,\tau)$ is used instead of $T(z,t)$ because the substrate is expected to attain a quasi-steady state temperature distribution within the laser-substrate interaction time τ as the laser beam passes over the substrate. The boundary and initial conditions for Eq. (6) are

$$C(0, t) = C_0, \quad (7a)$$

$$C(\infty, t) = 0, \quad (7b)$$

and

$$C(z, 0) = C_i(z), \quad (7c)$$

where C_0 and $C_i(z)$ are the dopant concentration at the substrate surface and the initial dopant concentration distribution in the substrate, respectively, which are obtained from the SIMS data for the doped samples. Assuming no Ga in the as-received sample and $C_1(z, 0)$, $C_2(z, 0)$ and $C_3(z, 0)$ as the Ga concentrations in the doped samples after the first, second and third laser passes, respectively, $C_i(z)$ can be expressed as follows for different number of laser passes

$$C_i(z) = 0 \quad \text{for the first pass}, \quad (8a)$$

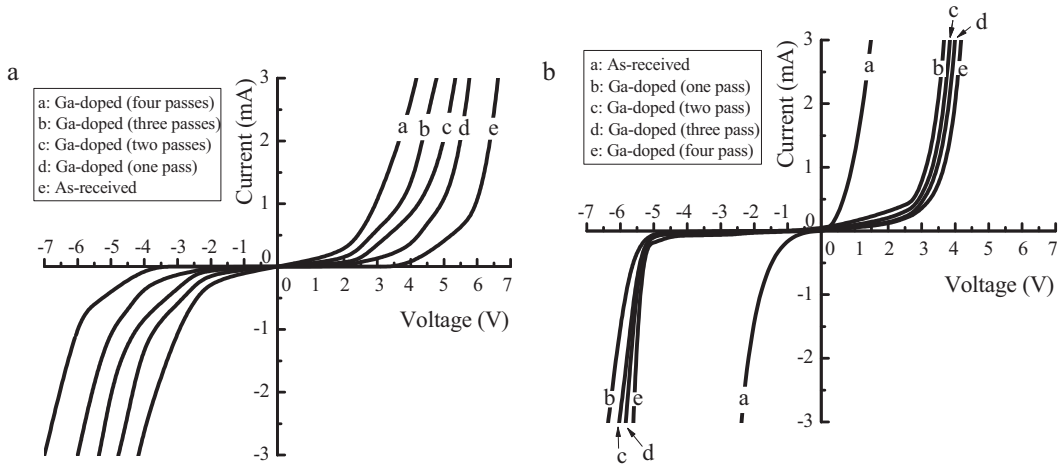

Fig. 4. Current–voltage plots for as-received n-type 4H–SiC sample and after the sample was doped with Ga (p-type dopant) under different numbers of laser passes: (a) measured on the same surface of the sample and (b) measured across the thickness of the sample with one probe on the p-doped side and the other probe on the parent n-type side.

$$C_i(z) = C_1(z, 0) \quad \text{for the second pass,} \tag{8b}$$

$$C_i(z) = C_2(z, 0) \quad \text{for the third pass,} \tag{8c}$$

and

$$C_i(z) = C_3(z, 0) \quad \text{for the fourth pass.} \tag{8d}$$

The Laplace transform of Eq. (6) yields

$$D_T(T(z,\tau))\frac{d^2\bar{C}(z,s)}{dz^2} + D_T'(T(z,\tau))\frac{d\bar{C}(z,s)}{dz} - \frac{s}{D_0}\bar{C}(z,s) = \frac{-C_i(z)}{D_0}, \tag{9}$$

where $D_T(T(z,\tau)) = e^{-Q/k_B T(z,\tau)}$ and $D_T'(T(z,\tau)) = dD_T(T(z,\tau))/dz$. Eq. (9) can be simplified (see Appendix A) to obtain the following expression for the dopant concentration distribution.

$$C(z,t) = \frac{1}{(D_T(T(z,\tau)))^{1/4}}\left[C_0(D_T(T(0,\tau)))^{1/4} erfc\left(\frac{L(z)}{2\sqrt{D_0 t}}\right) + \int_0^{L(\infty)} F_1(z')\left\{\frac{\exp(-(L(z')+L(z))^2/4D_0t) - \exp(-(L(z)-L(z'))^2/4D_0t)}{\sqrt{\pi t}}\right\}dz' + \int_0^{L(\infty)} F_2(z')I_{G1}dz' - \int_0^{L(\infty)} F_2(z')I_{G2}dz'\right], \tag{10}$$

where

$$I_{G1} = \frac{2}{\sqrt{\pi}}\left(C_i(z') + \frac{C(z',\tau) - C_i(z')}{\tau}t\right)\left[\sqrt{t}\exp\left\{-\frac{(L(z')+L(z))^2}{4D_0t}\right\} - \sqrt{\pi\frac{(L(z')+L(z))^2}{4D_0t}}erfc\left(\sqrt{\frac{(L(z')+L(z))^2}{4D_0t}}\right)\right] - \frac{2}{\sqrt{\pi}}\left(\frac{C(z',\tau) - C_i(z')}{\tau}\right)\left[\frac{2\sqrt{\pi}}{3}\left\{\frac{(L(z')+L(z))^2}{4D_0}\right\}^{3/2} erfc\left(\sqrt{\frac{(L(z')+L(z))^2}{4D_0t}}\right) + \frac{1}{2}\frac{\exp\left\{-(L(z')+L(z))^2/4D_0t\right\}}{t^{3/2}}\left\{\frac{2}{3} - \frac{4}{3}\frac{(L(z')+L(z))^2}{4D_0t}\right\}\right] \tag{11a}$$

and

$$I_{G2} = \frac{2}{\sqrt{\pi}}\left(C_i(z') + \frac{C(z',\tau) - C_i(z')}{\tau}t\right)\left[\sqrt{t}\exp\left\{-\frac{(L(z')-L(z))^2}{4D_0t}\right\} - \sqrt{\pi\frac{(L(z')-L(z))^2}{4D_0t}}erfc\left(\sqrt{\frac{(L(z')-L(z))^2}{4D_0t}}\right)\right] - \frac{2}{\sqrt{\pi}}\left(\frac{C(z',\tau) - C_i(z')}{\tau}\right)\left[\frac{2\sqrt{\pi}}{3}\left\{\frac{(L(z')-L(z))^2}{4D_0}\right\}^{3/2} erfc\left(\sqrt{\frac{(L(z')-L(z))^2}{4D_0t}}\right) + \frac{1}{2}\frac{\exp\left\{-(L(z')-L(z))^2/4D_0t\right\}}{t^{3/2}}\left\{\frac{2}{3} - \frac{4}{3}\frac{(L(z')-L(z))^2}{4D_0t}\right\}\right]. \tag{11b}$$

Eq. (10) is used to calculate the dopant concentrations at various depths by varying the values of D_0 and Q, and these two parameters are determined by reducing the error between the theoretical results and the SIMS data.

4. Results and discussion

4.1. Temperature distribution in SiC during laser doping

The temperature distribution in the substrate is calculated using Eq. (5) for various thermophysical properties listed in Table 1. The laser irradiance was varied to calculate the optimum temperature for laser doping by maintaining the substrate temperature below its melting temperature, which is the peritectic temperature of 3100 K for SiC, in this study. These calculations enable selecting the laser doping parameters to prevent any thermal damage and crystalline phase transformation of the substrate. Fig. 3 shows the temperature distribution at time $t = \tau = 0.25$ s over the entire thickness (375 μm) of the substrate. The maximum temperature is 2172 K at the surface for the case of doping with 4 laser passes and it gradually decreases due to cooling through heat dissipation along the thickness. Based on these calculations, the laser parameters were selected for carrying out the doping experiments as discussed in section 2. The laser irradiance at the substrate surface was 334.23 kW/cm^2.

4.2. Current–voltage (I–V) characteristics of the doped sample

The current–voltage characteristics of the sample were measured with a Tektronix 577 *I–V* curve tracer equipped with tungsten probes. Since the parent as-received sample was an n-type 4H–SiC substrate, which was doped with a p-type dopant Ga, a p–n junction is expected to form in the sample. The *I–V* characteristics of both the sample surface and p–n junction are presented in Fig. 4(a) and (b) respectively. The surface *I–V* characteristics are symmetric for the forward and reverse biases, indicating no p–n junction formed at the sample surface. Fig. 4(b), on the other hand, shows the typical p–n diode characteristics with large breakdown voltage in the reverse bias, while rapid increase in current for the forward bias.

Table 1
Properties of n-type 4H–SiC substrate with the optical properties at the wavelength of 1064 nm.

Absorption coefficient, μ (cm^{-1})[†]	45.73, 52.74, 53.01, 53.20
Reflectance of SiC substrate, R[†]	0.15, 0.14, 0.14, 0.13
Heat transfer coefficient, h (W/cm^2 K)	5
Thermal conductivity, k (W/cm K)	3.7
Thermal diffusivity, α (cm^2/s)	1.7
Thickness of substrate, d (μm)	375

[†] Four data are for the as-received, one-, two- and three-pass samples respectively.

The surface *I–V* characteristics were measured with the probes placed 1 mm apart on the silver contacts at the surface of each sample. While the symmetric *I–V* curves are due to the measurements of the surface characteristics, the nonlinear current responses could be due to Schottky contacts between the probes and sample. In the nonlinear regime where diffusion current dominates, the curves are parallel within the scope of experimental error, indicating that all of the samples have the same resistance. In the linear regime, however, the resistances for the as-received, one-pass, two-pass, three-pass, and four-pass samples are found to be 282, 31.3, 20.8, 8.33 and 4.55 kΩ, respectively, indicating that higher dopant concentration reduces the surface resistance. This trend could be due to the effect of the p–n junction beneath the surface with higher built-in potential at higher dopant concentrations, which may affect the flow of electrons from one probe to the other probe. Also higher dopant concentrations may affect the work function at the surface of the doped region, which can reduce the contact resistance between the sample surface and metal contact. For Fig. 4(b), the *I–V* characteristics were measured across the sample thickness with one probe in contact to the p-doped side and the other probe contacting the as-received n-type side. The results in this figure

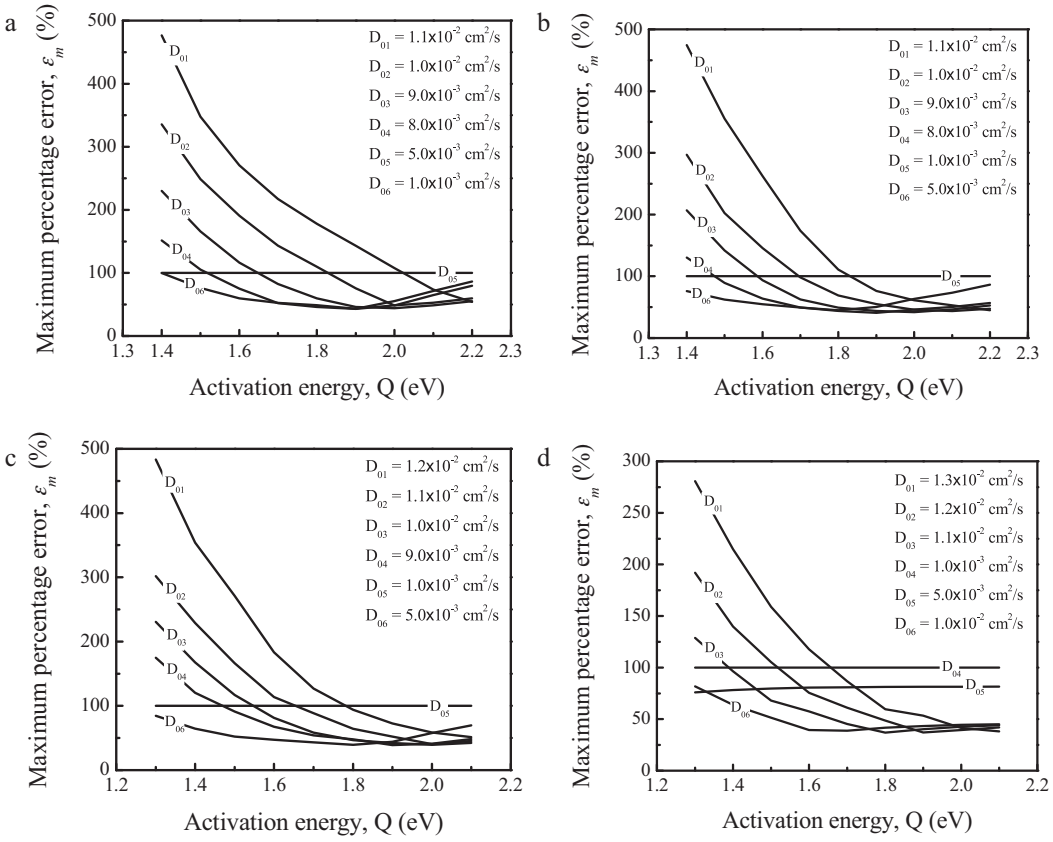

Fig. 6. Maximum error for different number of laser passes: (a) one-pass, (b) two-pass, (c) three-pass and (d) four-pass, showing ε_m for determining the values of Q and D_0.

indicate that the laser-doped Ga atoms were effective in forming p–n diodes of different *I–V* characteristics corresponding to different dopant concentrations. The *I–V* trend of the parent as-received sample indicates that the probes might form Schottky contacts with the sample.

4.3. Dopant profiles in SiC

Typical values of the Ga dopant concentration, which are obtained from the SIMS analysis, are presented in Fig. 5 for 4 laser passes. The original SIMS data of arbitrary units are converted to cm^{-3} using an ion-implanted n-type 4H–SiC standard, which was prepared by implanting Ga ions into the substrate with a dose of $10^{16}\,cm^{-2}$ at 150 keV. The concentration profile of the ion-implanted sample exhibits an increasing and then decreasing trends in the near- and far-surface regions, respectively, which differ from the monotonically decreasing trend of the profile obtained by laser doping. The concentration of Ga is found to be $6.25 \times 10^{20}\,cm^{-3}$ at the substrate surface, which exceeds its solid solubility limit ($1.8 \times 10^{19}\,cm^{-3}$) in SiC [27].

The ability to predict and control the dopant concentration profiles is important for the design and development of semiconductor and optoelectronic devices. Eq. (10) can be used to calculate the dopant profiles provided the temperature-dependent diffusion coefficient, particularly the values of Q and D_0, are known. These two diffusion parameters are determined in this study by comparing the experimental dopant profiles, i.e., the SIMS data, to the theoretical profiles obtained from Eq. (10) for different values of Q and D_0. The experimental dopant concentrations, $C_{ex}(z_i,\tau)$ for $i = 1, 2, 3, \ldots, N$, are obtained from the SIMS data at N different points along the depth of the substrate. The theoretical dopant concentrations, $C_{th}(z_i,\tau)$ for $i = 1, 2, 3, \ldots, N$, are calculated from Eq. (10) by substituting the temperature, $T(z_i,\tau)$, obtained from the thermal model of Eq. (5) and by selecting certain representative values of Q and D_0. The absolute percentage error between the experimental and theoretical results are calculated as $\varepsilon_i(Q, D_0) = \left|(C_{ex}(z_i, \tau) - C_{th}(z_i, \tau))/C_{ex}(z_i, \tau)\right| \times 100$ for each selected depth z_i and for different values of N such as $N = 10$, 15, 20. From these values of $\varepsilon_i(Q,D_0)$, the largest value is selected as the maximum percentage error $\varepsilon_m(Q,D_0)$ for a given set of Q and D_0 used for calculating $\varepsilon_i(Q,D_0)$. Then another set of Q and D_0 is selected to determine $\varepsilon_m(Q,D_0)$. The maximum percentage errors are plotted in Fig. 6(a–d) as a function of Q with D_0 as the parameter for each doped quadrant corresponding to a specific number of laser pass.

Good fitting can be obtained between the theoretical curves and the experimental dopant profiles by changing these two parameters. For $D_0 = 7.8 \times 10^{-3}\,cm^2/s$, the least value of the maximum error, ε_m, is found to be 50.73% for the one-pass doped quadrant with corresponding $Q = 1.9$ eV as shown in Fig. 6(a) and listed in Table 2. It can be seen in Table 2 that the values of Q and D_0 vary in the second decimal point onwards for reducing the value of ε_m from 50.73% to 42.9%, which do not affect the value of the diffusion coefficient significantly. For the cases of two-, three- and four-pass, the diffusion parameters Q and D_0 are obtained by determining the least value of the maximum error, ε_m, from Fig. 6(b–d), respectively, and listed in Table 2 with the corresponding diffusion coefficients. The surface temperature, $T(0,\tau)$, which is calculated from Eq. (5), is slightly higher for the case of four-pass than for one-pass. The temperature depends on two optical properties of the substrate, absorption coefficient and reflectance, which are affected by the dopant concentration in the substrate. To determine the optical properties such as the reflectance, transmittance, absorbance and absorption coefficient of the doped samples at the wavelength 1064 nm, a Nd:YAG laser of this wavelength was incident on the sample at a small incident angle. The incident, reflected

Table 2
Diffusion parameters of Ga in n-type 4H–SiC during laser doping.

Number of laser passes	Activation energy, Q (eV)	Pre-exponential factor, D_0 (cm^2/s)	Maximum error, ε_m (%)	Surface temperature, $T(0,\tau)$ (K)	Diffusion coefficient, D (cm^2/s)
1	1.9	7.8×10^{-3}	50.73	2168	2.99×10^{-7}
	1.91	7.83×10^{-3}	42.9	2168	2.87×10^{-7}
2	1.9	8.4×10^{-3}	48.35	2169	3.63×10^{-7}
	1.89	8.41×10^{-3}	40.65	2169	3.3×10^{-7}
3	1.9	9.4×10^{-3}	44.25	2171	3.23×10^{-7}
	1.88	9.43×10^{-3}	38.99	2171	4.25×10^{-7}
4	1.8	1.1×10^{-2}	46.98	2172	7.32×10^{-7}
	1.84	1.05×10^{-2}	36.81	2172	5.53×10^{-7}

and transmitted powers of the laser beam were measured with a power meter, which are denoted by P_i, P_r and P_t respectively. The reflectance, transmittance and absorbance are given by P_r/P_i, P_t/P_i and $(P_i - P_r - P_t)/P_i$ respectively. The absorption coefficient (μ) was calculated using the relation $\mu = (1/d)\ln(P_i - P_r/P_t)$ based on the Beer–Lambert law.

Since the dopant concentration increases as the number of laser passes increases, these two properties are different for the four samples. The absorption coefficients are 45.73, 52.74, 53.01 and 53.2 cm^{-1} for the as-received, one-, two- and three-pass samples, respectively, and the corresponding reflectances are 0.15, 0.14, 0.14 and 0.13 at 1064 nm wavelength. $T(0,\tau)$ is calculated using these optical properties assuming that the thermophysical properties of the substrate are not affected by the dopant concentration. The surface temperature and, consequently, the diffusion coefficient, increase due to the decrease in reflectance as the number of laser passes increases.

The values of Q and D_0 are listed in Table 2 for the maximum errors, i.e., $\varepsilon_m(Q,D_0) = 42.9\%$, 40.65%, 38.99% and 36.81% for one-, two-, three- and four-pass cases respectively. The maximum error is less for the case of four-pass than for one-pass. The activation energy, pre-exponential factor and diffusion coefficient are 1.84 eV, 1.05×10^{-2} cm^2/s and 5.53×10^{-7} cm^2/s at the substrate surface, respectively, for four-pass and the corresponding values are 1.91 eV, 7.83×10^{-3} cm^2/s and 2.87×10^{-7} cm^2/s for one-pass. The variation of diffusion coefficients is shown in Fig. 7 as a function of the substrate temperature for different laser passes. The diffusion coefficient has the highest value at the substrate surface and then it decreases linearly along the depth as the substrate temperature decreases, which may be due to more random vibrational motions of the Si, C and Ga atoms at high temperatures than at low temperatures. Another reason could be that the dopant atoms can diffuse by occupying the vacancies and interstitial sites created by laser irradiation and that the vacancy density decreases as the distance from the hottest point increases. It should be noted that the diffusion coefficient is higher for 4 laser passes than for 1 pass. This result may be explained by considering that a certain number of vacant and interstitial sites are created in each laser pass and a fraction of these sites is occupied by the dopant atoms during the pass. In the subsequent pass, the left-over sites from the previous pass and the newly created sites during the current pass contribute to the migration of the dopant atoms, causing enhanced diffusion coefficient as the number of laser passes increases.

Table 3
Surface concentration and diffusion lengths of Ga in n-type 4H–SiC substrate.

Number of laser passes	Surface concentration, $C(z,t)$ (cm^{-3})	Diffusion length, z (nm)
1	1.15×10^{19}	42
2	1.19×10^{20}	128
3	3.22×10^{20}	210
4	6.25×10^{20}	360

Based on the values of Q and D_0 obtained above, the theoretical Ga concentration distributions are calculated using Eq. (10) for different laser passes and compared to the experimental con-

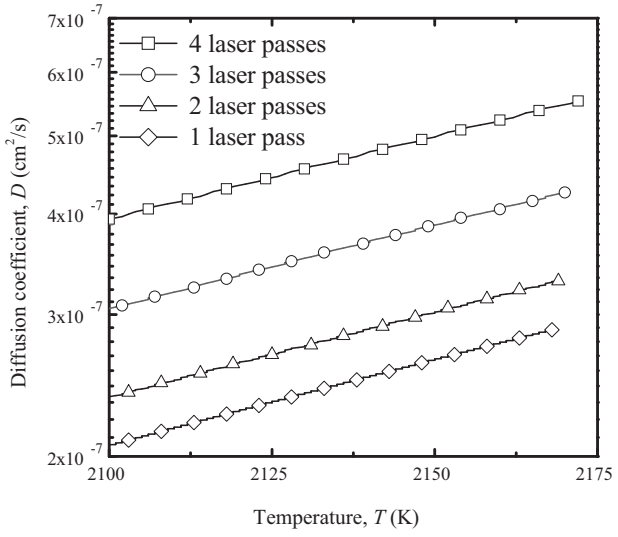

Fig. 7. Diffusion coefficients as a function of temperature for different number of laser passes.

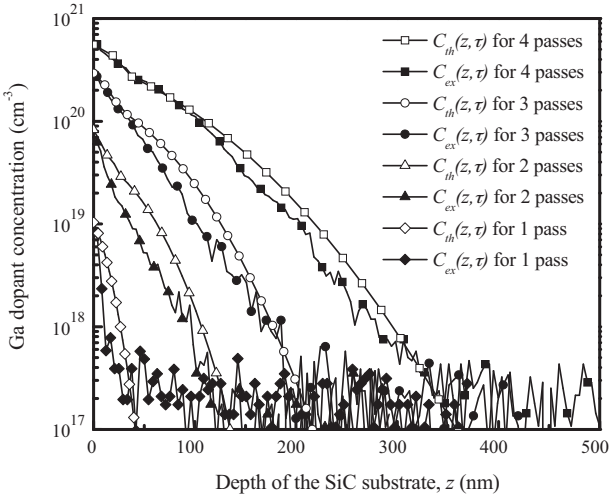

Fig. 8. Comparison of experimental (SIMS data) and calculated Ga concentration profiles for different number of laser passes.

centrations in Fig. 8. Although the theoretical results predict the same trend as the experimental data, the difference between the theory and experiment is small in the case of doping with 4 laser scans for which the maximum error, $\varepsilon_m(z_i,\tau)$, has the least value as indicated in Table 2. The surface concentrations and the diffusion lengths of Ga are listed in Table 3 for four different laser passes showing that the concentrations and the lengths increase as the number of passes increases. The concentration of Ga is about 1000 times higher at the substrate surface than at the end of the diffusion length inside the substrate, which may be due to the following effects. The presence of a surface partially relieves the stress caused by the mismatch in the atomic size of the dopant and matrix atoms, since the atoms are surrounded by certain types of atoms (Si, C and Ga) on one side of the surface and are exposed to different atoms of the ambient medium on the other side of the surface. Also there is a stress field near the surface due to atomic reconstruction and rapid cooling inherent in laser processing. These effects enhance the impurity solubility and diffusion causing high dopant concentrations near the surface [28].

The dopant atoms dissolve substitutionally in the SiC lattice by interacting with native point defects of interstitials or vacancies [29]. The vacancy concentration can be much higher during laser heating than when the substrate is at room temperature because of thermal diffusion in the steep temperature gradient (Soret effect) at the laser-heated surface, thermal stresses due to nonisothermal heating, laser-induced shock waves, electronic excitations and random vibrational motions of the atoms. Therefore the dopant concentration is generally high in the near-surface region. The enhanced diffusion coefficient and the increase in the surface concentration of Ga indicate that excess point defects of vacancies and interstitials are produced during laser doping.

5. Conclusion

Gallium was incorporated into n-type 4H–SiC substrate using a CW Nd:YAG laser for different number of laser scans. The laser parameters were selected using a thermal model to incorporate dopants without melting the substrate. Particularly solid-phase diffusion of Ga was achieved below the peritectic temperature of SiC. The surface *I–V* curves show that higher dopant concentrations reduce the resistance at the sample surface, while the bulk *I–V* characteristics across the sample thickness indicate the doped samples as p–n diodes. The surface concentration and the diffusion length of Ga are $6.25\times10^{20}\,\mathrm{cm}^{-3}$ and 360 nm respectively for the case of four laser passes, which are higher than the cases of fewer laser passes. Using the experimental Ga concentration, the activation energy, pre-exponential factor and diffusion coefficient were calculated by a method of parameter fitting based on a diffusion model involving temperature-dependent diffusion coefficient. The values of these diffusion parameters are 1.84 eV, $1.05\times10^{-2}\,\mathrm{cm}^2/\mathrm{s}$ and $5.53\times10^{-7}\,\mathrm{cm}^2/\mathrm{s}$, respectively, for the case of four laser passes. The diffusion coefficient is five orders of magnitude higher than the typical diffusion coefficient of Ga in SiC, which indicates that the laser doping process enhances the dopant diffusion coefficient significantly. Comparison of experimental and calculated dopant concentration profiles shows that they exhibit similar trends along the depth of the substrate.

Appendix A. Appendix

Defining the spatial and concentration variables as ξ and $\chi(\xi)$, respectively, by the following two expressions:

$$\xi = \int_0^z \frac{dz'}{\sqrt{D_T(T(z',\tau))}} = L(z) \tag{A1}$$

and

$$\chi(\xi) = \bar{C}(z,s)[D_T(T(z,\tau))]^{1/4}, \tag{A2}$$

Eq. (9) can be simplified as

$$\frac{d^2\chi(\xi)}{d\xi^2} - \frac{s\chi(\xi)}{D_0} = g(\xi), \tag{A3}$$

where $g(\xi) = -C_i(z)(D_T(T(z,\tau)))^{1/4}/D_0 - (D_T(T(z,\tau)))^{-1}(D_T'(T(z,\tau)))^2\chi(\xi)/16 + D_T''(T(z,\tau))\chi(\xi)/4$.

The solution of the ordinary differential Eq. (A3) subject to the boundary conditions 7(a) and 7(b)7(a) and (b) is given by

$$\begin{aligned}\bar{C}(z,s) &= (D_T(T(z,\tau)))^{-1/4}\left[C_0(D_T(T(0,\tau)))^{1/4}\frac{e^{-\sqrt{s/D_0}L(z)}}{s}\right.\\ &+\int_0^{L(\infty)}\frac{e^{-\sqrt{s/D_0}|L(z')-L(z)|}}{\sqrt{s}}F_1(z')dz' + \int_0^{L(\infty)}\frac{e^{-\sqrt{s/D_0}|L(z')-L(z)|}}{\sqrt{s}}F_2(z')\bar{C}(z',s)dz'\\ &-\int_{L(z)}^{L(\infty)}\frac{e^{-\sqrt{s/D_0}|L(z')-L(z)|}}{\sqrt{s}}F_1(z')dz' - \int_{L(z)}^{L(\infty)}\frac{e^{-\sqrt{s/D_0}|L(z')-L(z)|}}{\sqrt{s}}F_2(z')\bar{C}(z',s)dz'\\ &\left.-\int_0^{L(z)}\frac{e^{-\sqrt{s/D_0}|L(z')+L(z)|}}{\sqrt{s}}F_1(z')dz' - \int_0^{L(z)}\frac{e^{-\sqrt{s/D_0}|L(z')+L(z)|}}{\sqrt{s}}F_2(z')\bar{C}(z',s)dz'\right]\end{aligned} \tag{A4}$$

where

$$F_1(z') = -\frac{C_i(z')}{2\sqrt{D_0}(D_T'(T(z',\tau)))^{1/4}} \tag{A5a}$$

and

$$F_2(z') = \frac{\sqrt{D_0}}{2(D_T(T(z',\tau)))^{1/4}}\left\{\frac{1}{4}D_T''(T(z',\tau)) - \frac{1}{16}\frac{(D_T'(T(z',\tau)))^2}{D_T(T(z',\tau))}\right\}. \tag{A5b}$$

Here $D_T''(T(z',\tau)) = d^2D_T(T(z',\tau))/dz'^2$.

Taking the inverse Laplace transform of Eq. (A4) and applying the convolution theorem [30] to the integral terms that contain $\bar{C}(z',s)$ as a factor, the dopant concentration distribution can be obtained as given by Eq. (10).

References

[1] S. Lloyd, S. Savage, in: W.J. Choyke, H. Matsunami, G. Pensl (Eds.), Silicon Carbide, Springer, New York, 2004, pp. 27–55, pp. 179–205, 869–893.
[2] T. Kimoto, H. Matsunami, in: Z.C. Feng, J.H. Zhao (Eds.), Optoelectronic Properties of Semiconductors and Superlattices, Taylor & Francis, New York, 2004, pp. 2–40.
[3] M.S. Janson, M.K. Linnarsson, A. Hallen, B.G. Svensson, N. Nordell, H. Bleichner, Appl. Phys. Lett. 76 (2000) 1434–1436.
[4] G.J. Phelps, E.G. Chester, C.M. Johnson, N.G. Wright, J. Appl. Phys. 94 (2003) 4285–4290.
[5] I.O. Usov, A.A. Suvorova, V.V. Sokolov, Y.A. Kudryavtsev, A.V. Suvorov, J. Appl. Phys. 86 (1999) 6039–6042.
[6] A. Pokhmurska, O. Bonchik, S. Kiyak, G. Savitski, A. Gloskovsky, Appl. Surf. Sci. 154 (2000) 712–715.
[7] T. Akane, T. Nii, S. Matsumoto, Jpn. J. Appl. Phys. 31 (1992) 4437–4440.
[8] S. Matsumoto, S. Yoshioka, J. Wada, S. Inui, K. Uwasawa, J. Appl. Phys. 67 (1990) 7204–7210.
[9] E. Fogarassy, J. Venturini, in: J. Perriere, E. Millon, E. Fogarassy (Eds.), Recent Advances in Laser Processing of Materials, Elsevier, Oxford, 2005, pp. 375–409.
[10] W.L. Brown, in: M. Bass (Ed.), Laser Materials Processing, North-Holland Publishing Company, New York, 1983, pp. 339–406.
[11] S. Ahmed, C.J. Barbero, T.W. Sigmon, Appl. Phys. Lett. 66 (1995) 712–714.
[12] S.Y. Chou, Y. Chang, K.H. Weiner, T.W. Sigmon, J.D. Parsons, Appl. Phys. Lett. 56 (1990) 530–532.
[13] T. Mizunami, N. Toyama, Jpn. J. Appl. Phys. 37 (1998) 94–95.
[14] Y. Hishida, M. Watanabe, K. Sekine, K. Sugino, J. Kudo, Appl. Phys. Lett. 76 (2000) 3867–3869.
[15] T.F. Deutsch, J.C.C. Fan, G.W. Turner, R.L. Chapman, D.J. Ehrlich, R.M. Osgood, Appl. Phys. Lett. 38 (1981) 144–146.
[16] S. Kato, T. Nagahori, S. Matsumoto, J. Appl. Phys. 62 (1987) 3656–3659.
[17] T. Sameshima, S. Usui, M. Sekiya, J. Appl. Phys. 62 (1987) 711–713.
[18] J. Pezoldt, A.A. Kalnin, D.R. Moskwina, W.D. Savelyey, Nucl. Instrum. Methods Phys. Res. B 80 (1993) 943–948.

[19] A.G. Grigoryants, Basics of Laser Material Processing, CRC, Boca Ranton, 1994, pp. 69–126.
[20] Z. Tian, I.A. Salama, N.R. Quick, A. Kar, Acta Mater. 53 (2005) 2835–2844.
[21] Z. Tian, N.R. Quick, A. Kar, Acta Mater. 54 (2006) 4273–4283.
[22] S. Bet, N.R. Quick, A. Kar, Acta Mater. 55 (2007) 6816–6824.
[23] S. Bet, N.R. Quick, A. Kar, Acta Mater. 56 (2008) 1857–1867.
[24] C. Zhang, I.A. Salama, N.R. Quick, A. Kar, J. Appl. Phys. 99 (2006) 113530–113531.
[25] M.N. Ozisik, Heat Conduction, 2nd edition, John Wiley and Sons, New York, 1993, pp. 372–389.
[26] M.E. Glicksman, Diffusion in Solids: Field Theory, Solid-State Principles and Applications, John Wiley and Sons, New York, 2000, pp. 31–43, 175–182, 256–259.
[27] Y. Gao, S.I. Soloviev, T.S. Sudarshan, Appl. Phys. Lett. 83 (2003) 905–907.
[28] J. Tersoff, Phys. Rev. Lett. 74 (1995) 5080–5083.
[29] H. Bracht, N.A. Stolwijk, M. Laube, G. Pensl, Appl. Phys. Lett. 77 (2000) 3188–3190.
[30] A.D. Polyanin, A.V. Manzhirov, Handbook of Mathematics for Engineers and Scientists, Chapman & Hall/CRC, New York, 2007, p. 437.